Spectrochimica Acta Part A: Molecular and Biomolecular Spectroscopy 138 (2015) 579–584

Contents lists available at ScienceDirect

Spectrochimica Acta Part A: Molecular and Biomolecular Spectroscopy

journal homepage: www.elsevier.com/locate/saa

Synthesis, crystal structure, and properties of a 1-D terbium-substituted monolacunary Keggin-type polyoxotungstate

Pengtao Ma, Yanan Si, Rong Wan, Shaowei Zhang, Jingping Wang *, Jingyang Niu *

Key Laboratory of Polyoxometalate Chemistry of Henan Province, Institute of Molecular and Crystal Engineering, College of Chemistry and Chemical Engineering, Henan University, Kaifeng, Henan 475004, PR China

HIGHLIGHTS

- The 1-D linear chainlike framework.
- Lanthanide-substituted polyoxometalate.
- Terbium photoluminescent property.
- ESI-MS spectrum in solution.

GRAPHICAL ABSTRACT

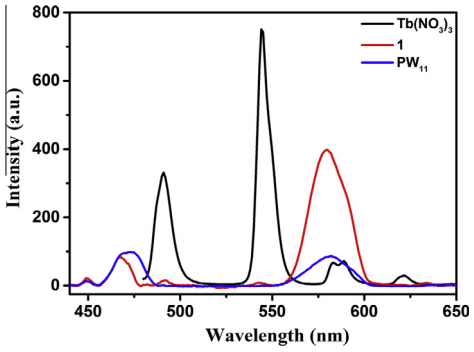

ARTICLE INFO

Article history:
Received 21 September 2014
Received in revised form 29 November 2014
Accepted 1 December 2014
Available online 9 December 2014

Keywords:
Polyoxotungstate
Lanthanide
Luminescent properties
ESI-MS spectrum

ABSTRACT

A new 1-D linear chainlike terbium-substituted polyoxometalate $[Tb(H_2O)_2(\alpha\text{-}PW_{11}O_{39})]^{4-}$ (**1**) has been synthesized in aqueous solution and characterized by elemental analysis, inductively coupled plasma atomic emission spectrometry (ICP-AES), X-ray powder diffraction (XRPD), IR spectrum, thermal analysis, electrospray ionization mass spectrometry (ESI-MS), and X-ray single-crystal diffraction. X-ray structural analysis reveals that **1** displays a 1-D linear chain containing $[Tb(H_2O)_2(\alpha\text{-}PW_{11}O_{39})]^{4-}$ moieties. The Tb(III) cation incorporated into the monolacunary Keggin-type $[\alpha\text{-}PW_{11}O_{39}]^{7-}$ unit resides in a distorted monocapped triangular prismatic geometry and acts as a linker to join two adjacent $[\alpha\text{-}PW_{11}O_{39}]^{7-}$ units to form a 1-D chain structure. Solid-state photoluminescent property of **1** has been investigated at room temperature and the photoluminescent emission mainly results from the synergistic effect of the Tb^{III} cation and the $Na_7[\alpha\text{-}PW_{11}O_{39}]$ precursor. The ESI-MS spectrum of **1** confirms that the polyanion $[Tb(H_2O)(HPW_{11}O_{39})]^{3-}$ is stable in aqueous solution.

Introduction

Currently, lanthanide(Ln)-substituted polyoxometalates (LSPs) have attracted increasing attention not only because polyoxometalates (POMs) have meaningful structural architectures and potential applications in various areas such as catalysis, nanotechnology, medicine and gas sorption [1–4], but also due to lanthanide (Ln) ions incorporated into POM frameworks showing interesting luminescence, magnetic and Lewis acid catalytic properties [5–7]. As we know, Ln cations display higher coordination numbers, stronger oxophilicity, and the inherent flexibility of the coordination geometries associated with their 4*f* electronic configurations relative to 3*d* transition metals, which are suitable for incorporating into POM frameworks to link POM fragments into multidimensional architectures. Also, Ln complexes usually represent

* Corresponding authors. Tel./fax: +86 371 23886876 (J. Niu).
E-mail addresses: jpwang@henu.edu.cn (J. Wang), jyniu@henu.edu.cn (J. Niu).

http://dx.doi.org/10.1016/j.saa.2014.12.001
1386-1425/

excellent luminescent behaviors resulting from *f–f* transitions [8,9]. Based on combination of the above-mentioned several aspects, the design and synthesis of LSPs with characteristic luminescence properties are of great interest for fundamental researchers. Therefore, considerable attention has been focused on exploring the reactions of Ln cations with lacunary POMs, and lots of various LSPs were continually reported. Firstly, in 1971, Peacock and Weakley reported that the reaction of Ln cations and monolacunary Keggin-type POMs $[XW_{11}O_{39}]^{n-}$ ($X = Si^{IV}$, P^{V}) led to the 1:1 and 1:2 derivatives, but no X-ray structural characterization was provided [10]. In 1987, a series of bis(undecatungstogermanate) lanthanates of potassium $K_{13}[Ln(GeW_{11}O_{39})_2]\cdot nH_2O$ (Ln = Ce, Pr, Nd, Sm, Eu, Gd, Tb, Dy, Tm, Yb) were prepared and characterized by Rong et al. [11]. Nevertheless, only 1:2-type such POM-based Ln derivatives were reported for decades. Until 2000, Pope et al. isolated two 1-D silicotungstates $[Ln(\alpha\text{-}SiW_{11}O_{39})(H_2O)_3]^{5-}$ ($Ln = Ce^{III}$, La^{III}), which represent the first infinite 1-D 1:1-type POM-based Ln derivatives [12]. Since then, LSPs were continuously exploited. In 2003, Mialane et al. expanded Pope's work and discovered another 1-D chainlike Ln-substituted silicotungstate $[Yb(\alpha\text{-}SiW_{11}O_{39})(H_2O)_2]^{5-}$ and a 2-D layer derivative $[Nd_2(\alpha\text{-}SiW_{11}O_{39})(H_2O)_{11}]^{2-}$ [13]. Subsequently, they prepared two 2:2-type dimers $K_{12}[\{(\alpha\text{-}SiW_{11}O_{39})Ln(COOCH_3)(H_2O)\}_2]$ (Ln = Gd^{III}, Yb^{III}) by the bridging role of CH_3COO^- [14]. In 2004, Nogueira et al. addressed a novel Ce^{IV}-substituted phosphotungstate $[Ce_2(PW_{10}O_{28})(PW_{11}O_{39})_2]^{17-}$ containing mixed $[PW_{11}O_{39}]^{7-}$ and $[PW_{10}O_{28}]^{11-}$ units [15]. In 2007, Kortz et al. communicated a series of 1:2-type β_2-Keggin silicotungstates $[Ln(\beta_2\text{-}SiW_{11}O_{39})_2]^{13-}$ (Ln = La^{III}, Ce^{III}, Sm^{III}, Eu^{III}, Gd^{III}, Tb^{III}, Yb^{III}) by reaction of Ln ions with the precursor $[\beta_2\text{-}SiW_{11}O_{39}]^{8-}$ [16]. In 2010, An et al. synthesized a family of lanthanide-substituted polyoxometaloborate composed of $[\{(H_2O)_4Ln(BW_{11}O_{39}H)\}_2]^{10-}$ (Ln = Ce^{III}, Nd^{III}) polyoxoanions with 3-D open frameworks [17]. Three years later, Wang et al. reported a group of 3-D metal–POM frameworks (MPFs) with two channels: $[Cu(enMe)_2]_{13}\{Ln(SiW_{11}O_{39})_2\}_2\cdot xH_2O$ (Ln = Ho^{III}, Dy^{III}, Eu^{III}, Er^{III}, Sm^{III}, Pr^{III}) [18].

Since 2004, our group has been exploiting the reactions of Ln cations with lacunary POM precursors and lead to a series of LSPs [19–26]. Among numerous reported LSPs, most of them are silicotungstates and germanotungstates, however, investigations of LSPs based on lacunary phosphotungstates are still relatively rare hitherto. In 2009, we began to concentrate on this branch and two kinds of 2:2-type dimeric lanthanophosphotungstates were isolated [24–26]. In this paper, we expect to discover LSPs with extended structures by the reaction of Ln cations with the $[\alpha\text{-}PW_{11}O_{39}]^{7-}$ precursor in conventional aqueous solution. Finally, a 1-D linear chainlike LSP $[(CH_3)_4N]_4[Tb(H_2O)_2(\alpha\text{-}PW_{11}O_{39})]\cdot 2H_2O$ (**1**) was successfully isolated. Interestingly, **1** exhibits a 1-D linear chain built by $[Tb(H_2O)_2(\alpha\text{-}PW_{11}O_{39})]^{4-}$ moieties, in which a distorted monocapped triangular prismatic Tb(III) cation is incorporated into the monolacunary Keggin-type building block. Solid-state photoluminescent property of **1** was investigated at room temperature and the ESI-MS spectrum of **1** was measured.

Experimental

Reagents and general techniques

$Na_7[\alpha\text{-}PW_{11}O_{39}]\cdot nH_2O$ was prepared as described and confirmed by IR spectrum [27]. Other chemicals are analytical grade used as purchased without purification. Elemental analyses (C, H, and N) were performed on a Perkin–Elmer 240C elemental analyzer. Inductively coupled plasma atomic emission spectrometry (ICP-AES) was performed on a Perkin–Elmer Optima 2000 ICP-AES spectrometer. IR spectra were obtained from a solid sample palletized with KBr on Bruker VERTEX 70 IR spectrometer in the range 400–4000 cm^{-1}. The TGA experiment was performed under N_2 atmosphere on a Mettler-Toledo TGA/SDTA851^e instrument with the heating rate of 10 °C min^{-1} from 25 to 1000 °C. The powder X-ray diffraction pattern was performed on a Bruker D8 ADVANCE instrument with Cu Kα radiation (λ = 1.54056 Å). Photoluminescence measurements were performed on HITACHI F-7000 fluorescence spectrophotometer. Electrospray ionization mass spectrometry (ESI-MS) routine spectra were carried out with a Bruker MTQ III-QTOF. The experiments were performed with the negative ion mode in mixed methanol/water (1:1) solvent by direct infusion with a syringe pump with a flow rate of 5 μL min^{-1}.

*Synthesis of $[(CH_3)_4N]_4[Tb(H_2O)_2(\alpha\text{-}PW_{11}O_{39})]\cdot 2H_2O$ (**1**)*

$Na_7[\alpha\text{-}PW_{11}O_{39}]\cdot nH_2O$ (1.40 g, 0.50 mmol) was dissolved in 15 mL distilled water at 80 °C, followed by dropwise addition of $Tb(NO_3)_3\cdot 6H_2O$ (0.59 g, 1.30 mmol) in 15 mL water. The resulting mixture was adjusted with 1 mol L^{-1} KOH solution to pH = 5.4 under stirring. After 1 h, the mixture was cooled to room temperature and the precipitate was removed by filtration. Then tetramethylammonium chloride (0.14 g, 1.46 mmol) was added. After 30 min, the resulting clear solution was filtered and left to evaporate at room temperature. Colorless block crystals of **1** were obtained after 2 weeks (Yield: *ca.* 38% based on W). IR (KBr pellet): 3450(w), 3040(m), 1630(m), 1480(s), 1097 (s), 1051(s), 951(s), 889(s), 823(w), 713(w), 592(m), 511(s). Elemental analysis (%) calcd for $C_{16}H_{56}N_4O_{43}PTbW_{11}$ (**1**): C, 6.00; H, 1.76; N, 1.75; P, 0.97; Tb, 4.96; W, 63.10. Found (%): C, 6.11; H, 1.82; N, 1.71; P, 0.94; Tb, 4.85; W, 63.33.

X-ray crystallographic determination

Intensity data for **1** were collected at 293(2) K using a Bruker Apex II CCD diffractometer with the graphite-monochromated Mo Kα radiation (λ = 0.71073 Å). Direct methods were used to solve the structure and to locate the heavy atoms using the *SHELXTL-97* program package [28,29]. The remaining atoms were found from successive full-matrix least-squares refinements on F^2 and Fourier syntheses. All of the non-hydrogen atoms were refined anisotropically. Positions of the hydrogen atoms connected to the carbon atoms were geometrically placed. All hydrogen atoms were refined isotropically. Hydrogen atoms were not included in the refinements. Crystallographic data and structure refinements for **1** are summarized in Table 1.

Results and discussion

Structural description

The experimental XRPD pattern of **1** is in agreement with the simulated XRPD pattern from the single-crystal X-ray diffraction, suggesting the good phase purity for **1** (Fig. 1). The differences in intensity between the experimental and simulated XRPD patterns may be due to the variation in preferred orientation of the powder sample during collection of the experimental XRPD pattern [30]. The bond valence sum calculations [31] indicate that the Tb, W and O atoms in **1** are in the +3, +6 and −2 oxidation states, respectively.

Single-crystal X-ray analysis reveals that **1** crystallizes in the monoclinic space group *P*2(1)/*c*, which comprises one mono-Tb^{III}-substituted phosphotungstate anion $[Tb(H_2O)_2(\alpha\text{-}PW_{11}O_{39})]^{4-}$, four $[(CH_3)_4N]^+$ countercations and two water molecules. Compound **1** exhibits a 1-D linear chain built by $[Tb(H_2O)_2(\alpha\text{-}PW_{11}O_{39})]^{4-}$ moieties, which is similar to that of $[M(GeW_{11}O_{39})$

Table 1
Crystallographic data and structure refinements for **1**.

	1
Empirical formula	$C_{16}H_{56}N_4O_{43}PTbW_{11}$
Formula weight	3204.89
Temperature (K)	293(2)
Wavelength (Å)	0.71073
Crystal system	Monoclinic
Space group	P21/c
a (Å)	13.361(10)
b (Å)	23.428(16)
c (Å)	22.520(12)
β (°)	115.72(3)
Z	4
Density (calculated) (g cm^{-3})	3.352
μ (mm^{-1})	21.043
Volume (Å^3)	6351(7)
F(000)	5672
Crystal size (mm^3)	0.24 × 0.22 × 0.17
θ range for data collection (°)	1.69–25.00
Limiting indices	$-12 \leqslant h \leqslant 15$, $-27 \leqslant k \leqslant 27$, $-26 \leqslant l \leqslant 15$
Reflections collected/unique	31,098/11,152 [*R*(int) = 0.1096]
Refinement method	Full-matrix least-squares on F^2
Data/restraints/parameters	11,152/104/668
GOF on F^2	1.001
Final *R* indices [$I > 2\sigma(I)$]	$R_1 = 0.0648$, $wR_2 = 0.1529$
R indices(all data)	$R_1 = 0.0958$, $wR_2 = 0.1662$
Largest diff. peak and hole (e Å^{-3})	3.148 and −3.165

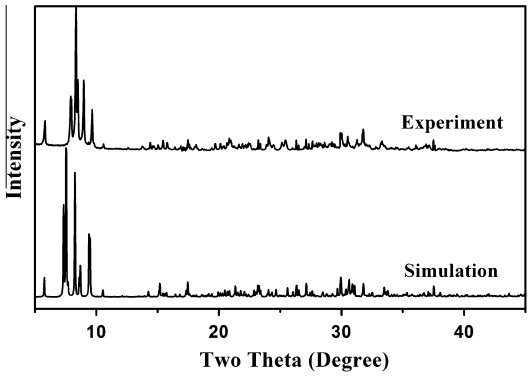

Fig. 1. Comparison of the simulated and experimental XRPD patterns of **1**.

$(H_2O)_2]^{5-}$ (M = Eu^{3+}, Tb^{3+}) [32]. As shown in Fig 2, the Tb1 cation is incorporated into the defect site of the polyanion $[\alpha\text{-}PW_{11}O_{39}]^{7-}$ and completes the saturated Keggin framework. The $Tb1^{III}$ cation adopts a seven-coordinate highly distorted monocapped trigonal prism geometry and is chelated by four O atoms from a monovacant polyanion $[\alpha\text{-}PW_{11}O_{39}]^{7-}$, one O atom from another adjacent polyanion $[\alpha\text{-}PW_{11}O_{39}]^{7-}$ and two water ligands (Fig. 2a and b). The Tb–O distances are in the range of 2.252(13)–2.400(17) Å. In the coordination configuration of the Tb1 cation, the O34, O35, O1W group and O25, O28, O2W group constitute two bottom surfaces of the trigonal prism with their dihedral angle of 3.7°, and the distances of the Tb1 cation and the two bottom planes are 1.552 and 1.282 Å, respectively. The O1W, O2W, O28, O35 group, O25, O28, O34, O35 group and O25, O34, O1W, O2W group form the three side planes of the trigonal prism and their standard deviations from their least-squares are 0.244, 0.004 and 0.244 Å, respectively. The distances between the $Tb1^{III}$ cation and the three side planes are 1.152, 1.002 and 0.431 Å, respectively. In addition, O7A (A: x, $-y + 1/2$, $z + 1/2$) occupies the cap position over the side plane defined by O25, O34, O1W, O2W group. The distance between O7A and the side plane defined by O25, O34, O1W, O2W group is 1.938 Å. The above-mentioned data indicate that the monocapped trigonal prism is severely distorted. Interestingly, the Tb^{3+} cations link these $[\alpha\text{-}PW_{11}O_{39}]^{7-}$ subunits into a 1-D linear chain (Fig. 2c) with $[N(CH_3)_4]^+$ cations around them to keep the charge balance. Such connection mode is obviously different from the 1-D chainlike Ce^{III}-based phosphotungstate derivative $[Ce(H_2O)_2(\alpha\text{-}PW_{11}O_{39})]^{4-}$ (**2**) [25]. There are three major distinctions between them: (i) $Tb1^{III}$ cation in **1** adopts a seven-coordinate monocapped trigonal prism geometry, whereas Ce1 atom in **2** is coordinated by eight oxygen atoms in a bicapped triangular prism environment [25]; (ii) every Tb^{3+} cation in **1** links to two $[\alpha\text{-}PW_{11}O_{39}]^{7-}$ subunits, but, every Ce^{3+} cation in **2** is connected with three $[\alpha\text{-}PW_{11}O_{39}]^{7-}$ subunits [25]; (iii) **1** exhibits a 1-D linear chain built by $[Tb(H_2O)_2(\alpha\text{-}PW_{11}O_{39})]^{4-}$ moieties, however, **2** displays the 1-D zigzag chain built by $[Ce(H_2O)_2(\alpha\text{-}PW_{11}O_{39})]^{4-}$ units [25].

Luminescent properties

Recently, the peculiar luminescent properties of Ln complexes can be exploited in versatile application areas such as biomedical, bio-sensing techniques, luminescence imaging, and so on [33]. As we known, Ln cations are usually observed weak sharp emission bands when directly excited, due to their low molar absorptivity and their 4*f* electrons [34,35]. When appropriate ligands can absorb and transfer the energy to Ln cations, the effective characteristic emission of Ln cations can be detected [36]. Thus, the photoluminescence spectrum of solid-state **1** has been collected at room temperature. When **1** was measured under excitation at 368 nm, characteristic luminescent bands were recorded at 448, 468, 492, 542, 580, and 633 nm (Fig. 3). In order to further investigate the source of luminescence, the solid-state photoluminescence spectra of $Na_7[\alpha\text{-}PW_{11}O_{39}]\cdot nH_2O$ and $Tb(NO_3)_3\cdot 6H_2O$ were measured at the same conditions (Fig. 3). Compared with the emission of the precursor $Na_7[\alpha\text{-}PW_{11}O_{39}]$, the luminescent bands at 448, 468 and 582 nm in **1** are evidently originated from the emission of the precursor $Na_7[\alpha\text{-}PW_{11}O_{39}]$, which may be attributed to the O → W transitions. The analogous intramolecular energy transfer from the O → W ligand-metal charge transition (LMCT) to Ln cations in POMs has been widely investigated by Yamase et al. [37,38]. It can be seen from the emission spectrum of $Tb(NO_3)_3$ in Fig. 3 that the characteristic low-intensity emission peaks at 491, 586, 622 nm and a high-intensity emission peak at 544 nm are ascribed to the $^5D_4 \rightarrow {}^7F_6$, $^5D_4 \rightarrow {}^7F_4$, $^5D_4 \rightarrow {}^7F_3$ and $^5D_4 \rightarrow {}^7F_5$ transitions of Tb^{III} cations, respectively. Thus, it's not difficult to determine that the luminescent bands at 492, 542, 580, and 633 nm of **1** correspond to the transitions to the ground-state ^7F_J (J = 6, 5, 4, 3) from the $^5D_4$ excited state of the Tb^{III} cation. However, it is interesting to observe the large decrease of luminescence intensity of emission peak at 542 nm, the possible reason of which is that the Tb^{III} cation is coordinated by two H_2O molecules resulting in the quenching of fluorescence, which is accord with the previous reports about terbium complexes [39,40]. In addition, the yellow emission at 580 nm is the most intense for **1**, which is related to the common interaction of O → W transitions and $^5D_4 \rightarrow {}^7F_4$ transitions, indicating that the $[\alpha\text{-}PW_{11}O_{39}]^{7-}$ ligand may be suitable for the sensitization of the yellow luminescence for Tb^{III} cations.

ESI-MS spectrum

The ESI-MS technique has been found to be a valuable analytic tool in studying the solution behavior of the nano-sized clusters, which has been extensively used to investigate many types of polyoxometalates [41,42]. Thus, the preliminary ESI-MS spectrum of **1** in mixed methanol/water (1:1) solvent was recorded in the negative ion mode, in order to confirm the identity of the cluster in the solution. As depicted in Fig. 4, the ESI-MS spectrum of **1** shows

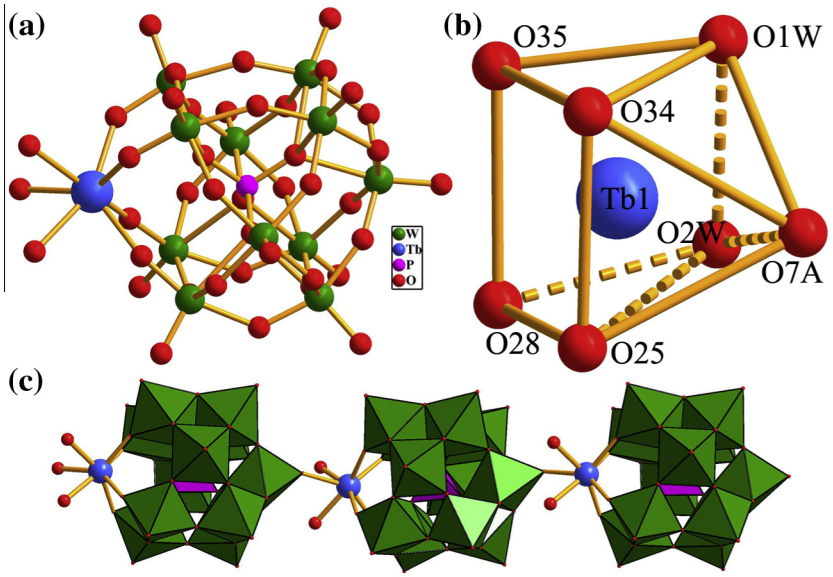

Fig. 2. (a) The ball-and-stick representation of the asymmetric polyanion unit of **1**; (b) the coordination environment of the $Tb1^{III}$ cation in **1**. The atoms with "A" in their labels are symmetrically generated (A: x, $-y+1/2$, $z+1/2$); (c) the 1-D linear chain structure of **1**. TMA cations and dissociative water molecules were omitted for clarity.

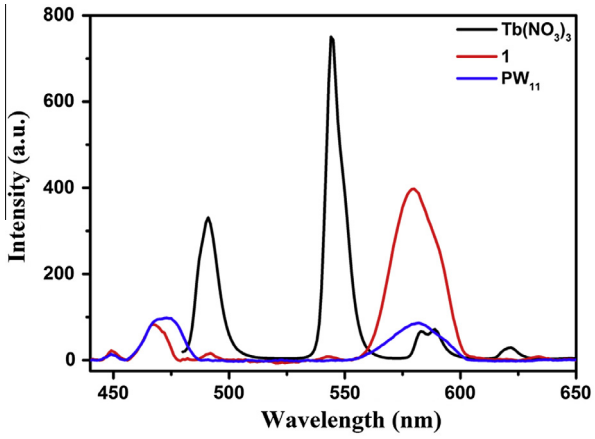

Fig. 3. The solid-state emission spectra for $Tb(NO_3)_3$ (black line), **1** (red line) and the precursor $Na_7[\alpha\text{-}PW_{11}O_{39}]$ (abbr. PW_{11}, blue line) at room temperature upon excitation at λ_{ex} = 368 nm. (For interpretation of the references to color in this figure legend, the reader is referred to the web version of this article.)

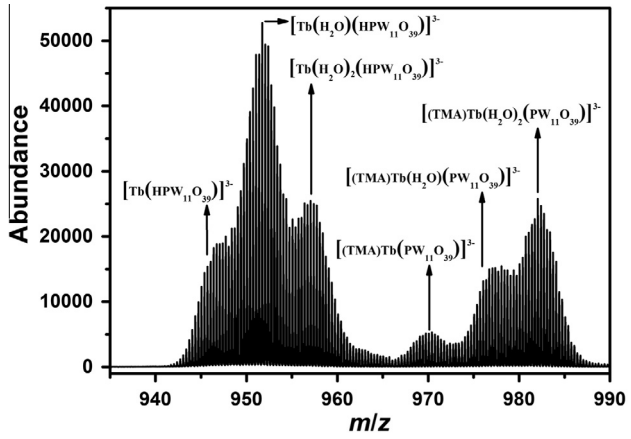

Fig. 4. Negative mode ESI-MS spectrum of **1** in mixed methanol/water (1:1) in the 935–990 m/z range.

a series of peaks for −3 charged ions appeared in the 940–990 m/z range, which correspond to those peak positions for $[Tb(H_2O)_n\text{-}PW_{11}O_{39}]^{4-}$ (n = 0, 1, or 2) adducts of protons or TMA cations. The composition of the polyanion leads to a wide isotopic Gaussian distribution nicely resolved owing to the high resolution of the mass analyzer, and the peak separations are differentiated by the number of combined charge-balancing TMA or protons and coordinated water molecules with the Tb^{III} cation. The highest intensity signal appears at m/z = 951.7, which is unambiguously attributed to the tricharged anion $[Tb(H_2O)(HPW_{11}O_{39})]^{3-}$, and two lower peaks on both sides appearing at 945.7 and 957.7 are assigned to the $[Tb(HPW_{11}O_{39})]^{3-}$ and $[Tb(H_2O)_2(HPW_{11}O_{39})]^{3-}$ polyanions. Additionally, another three lower peaks with m/z value of 970.1, 976.1 and 982.1 can be clearly attributed to the species $[(TMA)Tb(PW_{11}O_{39})]^{3-}$, $[(TMA)Tb(H_2O)(PW_{11}O_{39})]^{3-}$ and $[(TMA)Tb(H_2O)_2(PW_{11}O_{39})]^{3-}$, respectively. Assignments of these peaks show that **1** is observed as the assembly of $[TbPW_{11}O_{39}]^{4-}$ clusters with different numbers of cations and water molecules, showing some degree of stability in solution. The assignments indicate that the polyanion clusters retain their structural integrity in solution, which are in accord with the formulae derived from crystallographic analysis.

IR spectrum

The IR spectrum of **1** (Fig. 5) has been recorded between 4000 and 400 cm^{-1}, which is very useful for the identification of characteristic vibration bands of monolacunary Keggin polyanion and organic components in products. The characteristic vibration patterns derived from α-Keggin type polyanions are observed in 1100–700 cm^{-1}, which are in good agreement with the monolacunary Keggin-type polyanion. The vibration resonances at 1097 and 1051 cm^{-1}, are assigned to $\nu(P\text{–}O_a)$. The obvious characteristic bands appearing at 951, 889 and 823, 713 cm^{-1} are attributed to $\nu(W\text{–}O_t)$, $\nu(W\text{–}O_b)$, and $\nu(W\text{–}O_c)$, respectively. In addition, the ν(C–H) stretching band is observed at 3040 cm^{-1}, and the ν(C–N) stretching band appears at 1480 cm^{-1}, the vibration bands at 3450 and 1630 cm^{-1} are assigned to the stretching vibration ν(O–H) and bending vibration δ(O–H) of water molecules, respectively. The appearance of these characteristic signals confirms the

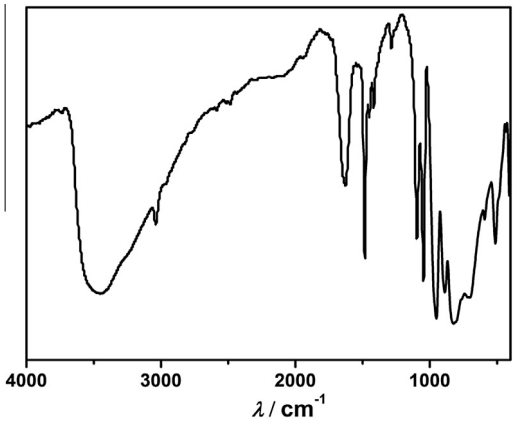

Fig. 5. The IR spectrum of **1**.

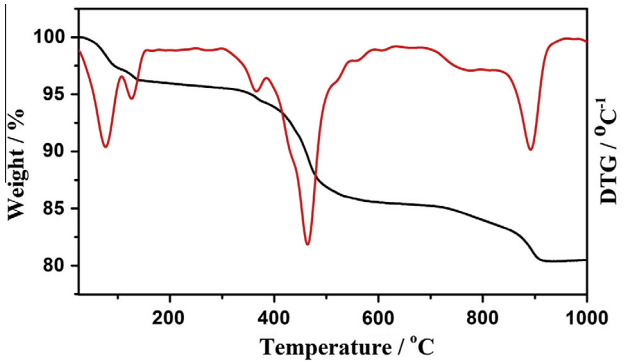

Fig. 6. TG and DTG curves of **1**.

presence of the $[(CH_3)_4N]^+$ cations and lattice water molecules, being good consistent with the single-crystal structural analysis results.

Thermal analysis

Thermal behavior of **1** has been studied by means of thermogravimetric (TG) and differential thermal gravity (DTG) measurements, which has been performed in the flowing N_2 atmosphere with a heating rate of 10 °C min^{-1} in the temperature region of 25–1000 °C. The TG and DTG curves (Fig. 6) indicate that the weight loss of **1** can be divided into three steps. The first weight loss of 4.1% occurred before 114 °C is assigned to the release of some adsorbed water molecules on the surface of the sample. Subsequently, two lattice water molecules and four tetramethylammonium groups are released in the second step up to 497 °C, and the observed weight loss of 10.6% is close to the calculated value of 10.4%. The third-step loss weight of 4.8% (calculated value of 4.3%) corresponds to the removal of two aqua ligands and the sublimation of phosphorus pentoxide together with the decomposition of the polyanion framework. In general, the second and the third step in the range of 114–1000 °C display two main steps of weight loss, which correspond to the release of H_2O, CO_2, N_2 and P_2O_5. Therefore, the final residues are probably a mixture of metal oxides (Tb_2O_3 and WO_3).

Conclusion

In summary, a 1-D Ln-substituted POM $[Tb(H_2O)_2(\alpha\text{-}PW_{11}O_{39})]^{4-}$ (**1**) based on lacunary $[\alpha\text{-}PW_{11}O_{39}]^{7-}$ building blocks has been successfully synthesized in aqueous solution. Interestingly, **1** exhibits a 1-D linear chain constructed from $[Tb(H_2O)_2(\alpha\text{-}PW_{11}O_{39})]^{4-}$ moieties, in which a distorted monocapped triangular prism Tb(III) cation is incorporated into the monolacunary Keggin-type $[\alpha\text{-}PW_{11}O_{39}]^{7-}$ units. The photoluminescence emission of **1** are mainly from the synergistic effect of the Tb^{III} cations and the $Na_7[\alpha\text{-}PW_{11}O_{39}]$ units. The ESI-MS spectrum of **1** confirms that the polyanion $[Tb(H_2O)(HPW_{11}O_{39})]^{3-}$ that is dissociated from **1** stabilizes in solution even at low concentration.

Acknowledgments

The authors thank the Natural Science Foundation of China (Nos. 21071042, 21171048, 21172052, 21201116), the Foundation of Education Department of Henan Province (Nos. 12A150004 and 14A150028) and Natural Science Foundation of Henan Province for financial support.

Appendix A. Supplementary data

CCDC 1015125 for **1** contains the supplementary crystallographic data for this paper. These data can be obtained free of charge via www.ccdc.cam.ac.uk/data request/cif, or from the Cambridge Crystallographic Data Center, 12 Union Road, Cambridge CB21EZ, UK (fax +44 1223 336 033, e-mail: deposit@ccdc.cam.ac.uk). Supplementary data associated with this article can be found, in the online version, at http://dx.doi.org/10.1016/j.saa.2014.12.001.

References

[1] M.T. Pope, Heteropoly and Isopoly Oxometalates, Springer-Verlag, Berlin, 1983.
[2] J.T. Rhule, C.L. Hill, D.A. Judd, Chem. Rev. 98 (1998) 327–357.
[3] A. Hiskia, A. Mylonas, E. Papaconstantinou, Chem. Soc. Rev. 30 (2001) 62–69.
[4] J.J. Borrás-Almenar, E. Coronade, A. Müller, M.T. Pope, Polyoxometalate Molecular Science, Kluwer Academic Publisher, Dordrecht, The Netherlands, 2004.
[5] X.F. Fang, T.M. Anderson, C. Benell, C.L. Hill, Chem. Eur. J. 11 (2005) 712–718.
[6] P. Mialane, A. Dolbecq, F. Sécheresse, Chem. Commun. (2006) 3477–3485.
[7] B.S. Bassil, M.H. Dickman, I. Romer, B. von der Kammer, U. Kortz, Angew. Chem. Int. Ed. 46 (2007) 6192–6195.
[8] J. Xia, B. Zhao, H.S. Wang, W. Shi, Y. Ma, H.B. Song, P. Cheng, D.Z. Liao, S.P. Yan, Inorg. Chem. 46 (2007) 3450–3458.
[9] D.T. de Lill, A. de Bettencourt-Dias, C.L. Cahill, Inorg. Chem. 46 (2007) 3960–3965.
[10] R.D. Peacock, T.J.R. Weakley, J. Chem. Soc. A (1971) 1836–1839.
[11] C. Rong, J. Liu, X. Chen, E. Wang, Inorg. Chem. Acta 130 (1987) 265–269.
[12] M. Sadakane, M.H. Dickman, M.T. Pope, Angew. Chem. Int. Ed. Engl. 39 (2000) 2914–2916.
[13] P. Mialane, L. Lisnard, A. Mallard, J. Marrot, E. Antic-Fidancev, P. Aschehoug, D. Vivien, F. Sécheresse, Inorg. Chem. 42 (2003) 2102–2108.
[14] P. Mialane, A. Dolbecq, E. Rivière, J. Marrot, F. Sécheresse, Eur. J. Inorg. Chem. (2004) 33–36.
[15] F.L. Sousa, F.A.A. Paz, A.M.V. Cavaleiro, J. Klinowski, H.I.S. Nogueira, Chem. Commun. (2004) 2656–2657.
[16] B.S. Bassil, M.H. Dickman, B. von der Kammer, U. Kortz, Inorg. Chem. 46 (2007) 2452–2458.
[17] H. An, Z. Han, T. Xu, Inorg. Chem. 49 (2010) 11403–11414.
[18] S. Yao, J.-H. Yan, H. Duan, Z.-M. Zhang, Y.-G. Li, X.-B. Han, J.-Q. Shen, H. Fu, E.-B. Wang, Eur. J. Inorg. Chem. (2013) 4770–4774.
[19] J.Y. Niu, M.L. Wei, J.P. Wang, D.B. Dang, Eur. J. Inorg. Chem. (2004) 160–170.
[20] J.Y. Niu, J.W. Zhao, J.P. Wang, Inorg. Chem. Commun. 7 (2004) 876–879.
[21] J.P. Wang, J.W. Zhao, X.Y. Duan, J.Y. Niu, Cryst. Growth Des. 6 (2006) 507–513.
[22] J.P. Wang, X.Y. Duan, X.D. Du, J.Y. Niu, Cryst. Growth Des. 6 (2006) 2266–2270.
[23] J.P. Wang, X.D. Du, Q.X. Yan, J.Y. Niu, J. Coord. Chem. 61 (2008) 3467–3475.
[24] J.Y. Niu, K.H. Wang, H.N. Chen, J.W. Zhao, P.T. Ma, J.P. Wang, M.X. Li, Y. Bai, D.B. Dang, Cryst. Growth Des. 9 (2009) 4362–4372.
[25] C. Zhang, P.T. Ma, H.N. Chen, J.P. Wang, J.Y. Niu, J. Coord. Chem. 64 (2011) 2178–2185.
[26] D.D. Zhang, C. Zhang, H.N. Chen, P.T. Ma, J.P. Wang, J.Y. Niu, Inorg. Chim. Acta 391 (2012) 218–223.
[27] C. Brevard, R. Schimpf, G. Tourne, C.M. Tourne, J. Am. Chem. Soc. 105 (1983) 7059–7063.
[28] G.M. Sheldrick, SHELXS97, Program for Crystal Structure Solution, University of Göttingen, Göttingen, Germany, 1997.

[29] G.M. Sheldrick, SHELXL97, Program for Crystal Structure Refinement, University of Göttingen, Göttingen, Germany, 1997.
[30] J.Y. Niu, S.W. Zhang, H.N. Chen, P.T. Ma, J.P. Wang, Cryst. Growth Des. 11 (2011) 3769–3777.
[31] I.D. Brown, D. Altermatt, Acta Crystallogr. B 41 (1985) 244–247.
[32] J.P. Wang, Q.X. Yan, X.D. Du, X.Y. Duan, J.Y. Niu, Inorg. Chim. Acta 361 (2008) 2701–2706.
[33] S.J.A. Pope, B.J. Coe, S. Faulkner, E.V. Bichenkova, X. Yu, K.T. Douglas, J. Am. Chem. Soc. 124 (2004) 9490–9491.
[34] P. Mahata, K.V. Ramya, S. Natarajan, Chem. Eur. J. 14 (2008) 5839–5850.
[35] J.J. Kido, Y.S. Okamoto, Chem. Rev. 102 (2002) 2357–2368.
[36] B.D. Chandler, J.Q. Yu, D.T. Cramb, G.K.H. Shimizu, Chem. Mater. 19 (2007) 4467–4473.
[37] T. Yamase, Handb. Phys. Chem. Rare Earths 39 (2009) 297–356.
[38] T. Yamase, Chem. Rev. 98 (1998) 307–325.
[39] A.A. Mamykin, A.V. Mamykin, S.S. Ostakhov, V.P. Kazakov, High Energy Chem. 44 (2010) 109–112.
[40] A.H. Yang, J.Y. Zou, W.M. Wang, X.Y. Shi, H.L. Gao, J.Z. Cui, B. Zhao, Inorg. Chem. 53 (2014) 7092–7100.
[41] H.N. Miras, E.F. Wilsonw, L. Cronin, Chem. Commun. (2009) 1297–1311.
[42] J.H. Son, C.A. Ohlin, R.L. Johnson, P. Yu, W.H. Casey, Chem. Eur. J. 19 (2013) 5191–5197.